(12)

NAVSWC TR 90-268

# PULSE SHAPING A HIGH-CURRENT RELATIVISTIC ELECTRON BEAM IN VACUUM



BY J. D. MILLER, R. F. SCHNEIDER, AND H. S. UHM (NAVSWC),
K. T. NGUYEN AND K. W. STRUVE (MISSION RESEARCH CORPORATION),
AND D. J. WEIDMAN (ADVANCED TECHNOLOGY AND RESEARCH)

RESEARCH AND TECHNOLOGY DEPARTMENT

28 JUNE 1990




NAVAL SURFACE WARFARE CENTER

Dahlgren, Virginia 22448-5000 • Silver Spring, Maryland 20903-5000

# PULSE SHAPING A HIGH-CURRENT RELATIVISTIC ELECTRON BEAM IN VACUUM

BY J. D. MILLER, R. F. SCHNEIDER, AND H. S. UHM (NAVSWC),
K. T. NGUYEN AND K. W. STRUVE (MISSION RESEARCH CORPORATION),
AND D. J. WEIDMAN (ADVANCED RESEARCH AND TECHNOLOGY)
RESEARCH AND TECHNOLOGY DEPARTMENT

28 JUNE 1990





NAVAL SURFACE WARFARE CENTER
Dahlgren, Virginia 22448-5000 • Silver Spring, Maryland 20903-5000

# FOREWORD

A simple method for shaping the output current pulse of a relativistic electron beam in vacuum is presented. This method has been employed to sharpen the risetime of a high-current relativistic electron beam produced by a 2 MV, 7 kA, 20 ns pulser. The beam nominally has a pulse shape that is triangular both in voltage and current, with a negligible instantaneous energy spread. The desired pulse shape is nominally rectangular in current. The technique utilizes a magnetic lens with a magnitude of approximately 1.5 kG to focus the beam. Passing beam electrons through the magnetic lens causes them to focus at different axial locations downstream from the lens depending upon their energy. The focal point of the beam current peak (corresponding to maximum energy) is then located furthest downstream. An aperture is used near the focus to select a portion of the beam having the desired parameters.

The authors would like to thank W. Freeman and M. Moffatt for technical assistance. This work was supported by the Strategic Defence Initiative Organization under funding document number N0001490WX15505 and Independent Research funds at the Naval Surface Warfare Center.

Approved by:

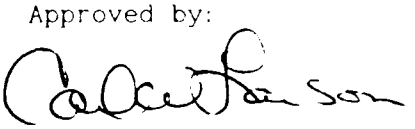

CARL W. LARSON, Head
Radiation Division

CONTENTS



ILLUSTRATIONS

# SECTION 1

# INTRODUCTION

Shaping the output current pulse of intense relativistic electron beam (IREB) generators is of interest for a variety of applications. Typically, a monoenergetic current pulse with a square profile, i.e., fast risetime and falltime and a relatively constant current level, is desirable. The output of many IREB generators is often sinusoidal or triangular with the current waveform shape following the diode voltage waveform. Consequently, the beam current risetime has an energy ramp associated with it. The problem of achieving a fast risetime when driving a highly capacitive load with a highly inductive Marx generator is a common one.

Various techniques have been proposed for beam risetime sharpening and current pulse shaping. These include inductive erosion of the electron beam,[1] vacuum surface flashover switches placed appropriately between the large Marx inductance and the vacuum diode,[2] and gradient B drift transport of the electron beam.[3,4] Since the beam risetime possesses an energy ramp, the possible use of a magnetic lens to sharpen the beam risetime is an attractive alternative due to its compactness and simplicity. In this report we discuss such an approach using a single magnetic lens.

It is a well-known fact that the focal point for relativistic electrons with kinetic energy $(\gamma-1)mc^2$ is given in the thin lens approximation by[5]

$$f = \frac{1}{\int \left( \frac{\omega_c}{2\gamma v_z} \right)^2 dz} \quad , \tag{1}$$

where $\omega_c(z) = eB/m$ is the electron cyclotron angular frequency, $v_z$ is the electron axial velocity, and $B_z(r,z)$ is the lens axial magnetic field profile along the electron path. Passing beam electrons through a magnetic lens will

cause the beam electrons to focus at different axial locations downstream from the lens, with the focal point of the beam current peak (corresponding to maximum energy) furthest downstream.

Thus, by placing a small aperture near the beam peak focal point, we can let the portion of the beam near peak pass through, while intercepting most of the early portion of the pulse which has spread out before it reaches the aperture. Similarly, the later portion of the pulse fall time will also be intercepted. This creates an electron beam with sharper rise and fall times resulting in a more uniform current profile.

The above description, while providing a simple scenario for the single particle case, is inadequate since it neglects several important factors. These factors include lens aberrations due to nonlinearity, beam space charge effects, and beam transverse energy. We shall discuss some of these issues in this report.

The report proceeds as follows. In Section 2 we present a description of the magnetic lens and its magnetic field profile. The theoretical basis for the current pulse shaping technique is discussed in Section 3. Included is the theoretical analysis and scaling laws for the risetime sharpener utilizing a foilless diode geometry. Results of numerical simulations using MAGIC are in good agreement with theory and show the potential for this approach. Diode geometries including an anode foil are also presented. Section 4 describes the experimental setup. The experimental results are presented and discussed in Section 5, while conclusions and recommendations are contained in Section 6.

## SECTION 2

## MAGNETIC LENS

As can be seen from Equation (1), the focal length for a magnetic lens depends not only on the peak axial magnetic field strength but also on the axial field profile. Therefore, in this section we describe the field profile of the lens to be used in the experiment.

The basic elements of a magnetic lens include a circular current-carrying coil and a yoke enveloping most of the coil surface area except for a small gap centered at the coil midplane and running along the coil inner bore circumference as shown in Figure 1(a). The yoke is manufactured with materials of very high magnetic permeability (e.g. soft iron) so that most of the magnetic flux is confined within the yoke itself. Without the presence of the gap, there would be very little field outside of the yoke. The presence of the gap allows the field to escape forming an azimuthally symmetric magnetic field which peaks axially at the coil midplane. This configuration is necessary so that the field can be confined to the shorter axial extent necessary to produce a thin lens out of bulky solenoidal coils.

The coil itself is a circular disk of 12 cm width, 12 cm inner bore radius, and 24 cm outer radius. The yoke is composed of high magnetic permeability steel and is 1.8 cm in thickness with a 5 cm gap. The measured axial field profile along the axis of symmetry, z, is shown in Figure 1(b). The magnetic field strength can be adjusted experimentally by varying the coil current (supplied by a dc power supply). The present coil can produce a 3-kG peak magnetic field on axis in the absence of the yoke.

The knowledge of the magnetic field profile on the axis of symmetry is essential in determining the field profile at other positions.[6] These are given by

$$B_z(r,z) = B(z) - \frac{1}{4} B''(z)r^2 + \ldots \tag{2a}$$

$$B_r(r,z) = -\frac{1}{2} B'(z)r + \frac{1}{16} B'''(z)r^3 + \ldots \tag{2b}$$

Here, the primes denote derivatives with respect to z. We note here that from Equations (1) and (2) it can be seen that particles traversing the lens at different radial distances from the axis of symmetry will have different focal lengths, even with the same kinetic energy. This aberration is a natural consequence of the nonlinearity of the magnetic field profile and it limits the smallest spot size to which a beam can be focused. Further, it also introduces nonlinearity into the particle radial momentum which is irreversible.

We have approximated the field profile on axis, as shown in Figure 1(b), by the following analytical expression,

$$B(z) = B_o e^{-\left( \frac{z-z_c}{z_o} \right)^2}, \tag{3}$$

where $B_o$ is the peak field strength on axis, $z_c$ is the axial position of the lens center, and $z_o = 7.7$ cm. This expression will be used in subsequent analysis in the following sections. For now we note that a useful integral formula for the field profile given above is

$$\int_{-\infty}^{\infty} B^2(z)dz = 1.8 B_o^2 z_o . \tag{4}$$

## SECTION 3

## CURRENT PULSE SHAPING WITH A MAGNETIC LENS

Typical high-power vacuum diode configurations consist of a cylindrical cathode shank with a flat emission surface and a thin foil acting as an anode a short distance downstream from the cathode surface. Some of the cathode materials utilized in high power diodes of this type include fine grain graphite or velvet. Velvet cathode surfaces have been observed experimentally to produce more uniform, lower transverse energy spread (lower emittance) beams than is possible with a graphite cathode.[7] Minimizing the transverse energy spread is an important consideration for many electron beam applications.

The presence of the anode foil introduces two issues which complicate the use of a single magnetic lens for current pulse shaping. One is that the foil will increase the beam emittance through scattering. Since the mean-squared scattering angle $\langle\theta^2\rangle$ of a relativistic electron after passing through scattering materials is proportional to $\gamma^{-2}$, the low-energy portion of the beam pulse will gain substantially more transverse energy relative to the beam peak. This limits the smallest spot size to which the beam peak can be focused.

The second issue is mainly applicable to the high-current beam case such as considered here. In the proximity of the foil the beam self-radial electric field is shorted out, leaving the self-azimuthal magnetic field which focuses the beam. Since the self-azimuthal magnetic field is proportional to beam current, this field can be on the order of 1 kG at the outer edge of the beam peak resulting in strong focusing prior to magnetic lens focusing. Due to the fact that the beam risetime possesses both current and energy ramps, foil focusing at the anode will, at the very least, complicate the experimental design. This phenomenon has been observed experimentally[8] and has been proposed as an alternative for high-current electron beam transport.[9,10]

These two issues may be avoided if the diode is operated in a foilless configuration. We will discuss separately the effectiveness of the magnetic lens in current pulse shaping in both diode configurations.

The general envelope equation for relativistic electron beam transport after the anode aperture in an axial magnetic field including space charge and emittance effects can be expressed by[5]

$$R'' - \frac{K}{R} - \frac{\varepsilon_n^2}{\gamma^2 R^3} + \left( \frac{\omega_c}{2\gamma v_z} \right)^2 R = 0 \tag{5}$$

Here, $K = 2eI_b/4\pi\epsilon_o m\beta^3 c^3 \gamma^3$ is the generalized beam perveance, $I_b$ is the beam current, $\varepsilon_n = \gamma\beta\delta\theta R$ is the beam normalized emittance which is a constant of motion in the absence of any nonlinear external force, $\delta\theta$ is the beam transverse thermal spread angle and R is the beam radius. Equation (5) assumes the beam energy is constant and the diode is a magnetic field free region. The magnetic field profile is as given by Equation (3) with the distance between the lens center and anode defined as $z_c$. Equation (5) can be integrated with the initial conditions, $R(z=0) = a$, and $R'(z=0) = r'_o$, to give

$$R'(z) = \left[ 2K\ell n\left(\frac{R}{a}\right) + \frac{\varepsilon_n^2}{\gamma^2 a^2}\left(1 - \frac{a^2}{R^2}\right) - \int_0^z \left(\frac{\omega_c}{2\gamma v_z}\right)^2 \frac{dR^2}{dz} dz + (r'_o)^2 \right]^{1/2} \tag{6}$$

and

$$R(z) = \int_0^z R'(z')dz' \tag{7}$$

Equation (5) or its equivalent, Equation (6), can be evaluated numerically to provide the beam radial envelope and its slope at any axial location z downstream from the anode.

## 3.1 NONMAGNETIZED FOILLESS DIODE

In this section we will investigate the radial phase space properties of an electron beam emerging from a nonmagnetized foilless diode configuration.[11] The radial impulse due to an aperture in an otherwise uniform anode plane (see Appendix for details) is

$$r' = \frac{v_r}{v_z} = \frac{eV}{\gamma m v_z^2}\frac{r}{2d} = \frac{\gamma}{\gamma+1}\frac{r}{2d} \tag{8}$$

It is interesting to note that r′ is linear in r and is independent of the aperture radius in this limit, providing d > a. Here d is the diode anode-cathode gap spacing and a is the anode aperture radius. In other words, the anode aperture acts as a negative lens[5] which preserves the beam laminarity. Furthermore, there is a weak dependency of r′ on energy resulting from the anode aperture which will advantageously lengthen the spacing between the focal points of the beam rising edge and the beam peak after passing through the magnetic lens. This information determines the beam initial conditions upon entering the lens region. With this knowledge, we can estimate the magnetic field strength required as well as the location for the downstream aperture.

Several observations can be made which greatly simplify the analysis of Equation (5) and allow simple formulae which are useful in estimating experimental and simulation parameters. First, the effect due to the magnetic lens focusing is proportional to $B^2(z)$, and B(z) peaks strongly at the center of the lens. Thus, by making use of Equation (4) we can reasonably approximate the lens magnetic field axial profile in the paraxial approximation as

$$B(z) = \begin{cases} B_o & , \; z_c - 0.9z_o \le z \le z_c + 0.9z_o \\ 0 & , \; \text{elsewhere} \; . \end{cases} \tag{9}$$

Here, z is defined as the distance from the anode. Second, with a beam peak current of several kiloamperes and an operating peak energy of about 2 MeV, space charge effects are negligible in comparison with the slope caused by the anode aperture. Thus, we can safely neglect the effect of space charge except for the region near the focal point where R<<a. Third, in the absence of the anode foil, most of the emittance is expected to come from the cathode surface roughness. An analytical formula[12] for angular spread $\delta\theta$, which was confirmed experimentally[7] is given by

$$\delta\theta \simeq \frac{0.1}{\gamma}\left( J_c h^2 \right)^{1/3} \tag{10}$$

where $J_c$ is the cathode current density and h is the height of the cathode whiskers. Taking h to be typically 30 μm for a velvet cathode[7] and assuming

the diode current to be 7 kA at peak voltage of 2 MeV for a 1 cm cathode radius and 2 cm diode gap spacing, we obtain $\delta\theta \simeq 5.2\times10^{-3}$ radians. Here again the effect due to cathode surface roughness is also expected to be negligible relative to the lensing effect of the anode aperture, i.e., $\delta\theta << r_o'$.

Making use of these observations, we can readily solve Equation (5) to obtain

$$R(z) = \begin{cases} r_o' z + a , & 0 \le z \le z_1 \\ r_1 \cos\left[k\left(z-z_1\right)\right] + \dfrac{r_o'}{k} \sin\left[k\left(z-z_1\right)\right] , & z_1 \le z \le z_2 \\ r_2 + r_2'\left(z-z_2\right) , & z \ge z_2 \end{cases} \tag{11}$$

and

$$R'(z) = \begin{cases} r_o' , & 0 \le z \le z_1 \\ -kr_1 \sin\left[k\left(z-z_1\right)\right] + r_o' \cos\left[k\left(z-z_1\right)\right] , & z_1 \le z \le z_2 \\ r_2' , & z \ge z_2 \end{cases} \tag{12}$$

where $z_1 = z_c - 0.9z_o$, $z_2 = z_c + 0.9z_o$, and the subscripts 1 and 2 denote the beam properties at these points, respectively. We have also defined $k = \omega_{co}/2\gamma v_z$. Thus, the axial location for the focal point can be readily estimated from Equation (12) to be

$$z_f = z_2 - \frac{r_2}{r_2'} . \tag{13}$$

Of course, the field strength must be sufficiently strong so that $r_2' < 0$ for the lens to be effective. Near this focal point, the beam radius does not go to zero but rather to a waist ($R'=0$). The radius at this point, $R_m$, can be determined from

$$2K\ell n\left(R_m/a\right) + \frac{\varepsilon_n^2}{\gamma^2 a^2}\left(1 - \frac{a^2}{R_m^2}\right) = -\left(r_2'\right)^2 \tag{14}$$

For a high-energy, low-emittance beam and a strong magnetic lens, Equation (14) indicates the beam can be focused to a very small spot.

The above analysis, while it explains the beam behavior in passing

through a perfect lens, unfortunately does not take into account the nonlinearity that is present in all real lenses; that is, it fails to account for nonlinear terms in Equation (2). Due to nonlinearity, the outer electrons will feel a slightly stronger bending force. Thus, they approach the symmetry axis at an enhanced rate from that predicted by linear analysis and miss the small waist where space charge and emittance effects are dominant. Consequently, these particles lose relatively little momentum and are expected to cross the axis of symmetry. In other words, magnetic lens nonlinearity introduces a high transverse energy component to an initially cool beam. This phenomenon may provide an explanation for the observed core-halo formation in transport experiments where magnetic lenses are employed in matching electron beams to focusing channels.

In order to verify the basic concept, we have performed numerical simulations with the MAGIC code.[13] MAGIC is a two-and-one-half dimensional, fully self-consistent particle-in-cell code developed by Mission Research Corporation to investigate axisymmetric plasma physics phenomena such as the one presented here. The basic geometry of the simulation includes the foilless diode and the magnetic lens region as shown in Figure 2.

The cathode emission surface has a radius of 1 cm, and we have set the critical electric field for cathode explosive field-emission initiation at the typical value of 200 kV/cm. The anode is 2.7 cm downstream from the cathode with an aperture of 1.2 cm in radius. The diode voltage is assumed to have the following temporal profile,

$$V_d(t) = V_p \sin\left(\frac{\pi t}{\tau_p}\right), \qquad t \le \tau_p \tag{15}$$

where we have set the peak voltage to be 2.2 MV, and the pulselength $\tau_p$ has been set at 37 ns for consistency with the observed voltage pulselength of the Febetron 705 electron beam generator used in the experiments. We have simulated the first 20 ns of the voltage pulse. The maximum cathode emission current density has been set at $2.5 \times 10^3$ A/cm$^2$ to yield a peak current of 7.9 kA as observed experimentally for velvet cathode and anode foil Febetron operation at this peak voltage. The diode current follows the sinusoidal shape of the diode voltage with a risetime (10-90%) of 11 ns.

The thermal spread angle due to cathode surface nonuniformity is on the order of $5 \times 10^{-3}$ radians, which is negligible compared to the anode aperture lensing effect. Equation (8) predicts the slope for the outermost electrons after passing through the anode aperture to be 0.18 radian at the peak voltage of 2.2 MV. Due to the weak energy dependence of the slope, a slight reduction of the beam risetime is expected upon passage through the aperture. This can be observed in Figure 3(a) which shows the beam current downstream from the anode. We note here that the discontinuities seen in Figure 3(a) are an artifact of all particle codes in statistically representing a large number of physical particles by a much smaller number of macro-particles.

The peak current of the apertured beam upon entering the magnetic lens cell is about 4.5 kA. The magnetic field profile in this region is as given by Equations (2) and (3) with $z_c$ = 18 cm measured downstream from the anode. The peak magnetic field has been arbitrarily chosen to be 1.7 kG. Using Equation (13), we estimate the focal point for the beam peak to be about 40 cm downstream from the anode. Therefore, we have placed the pulse shaping aperture at this location. In this run, the aperture is 1.8 cm in radius.

The simulated particle trajectory plots at different times in the beam pulse are shown in Figures 2(a)-(c). These plots are equivalent to snap shots at different times of the system. At early times, the beam is strongly focused by the lens due to low energy and is mostly intercepted by the aperture. In fact, if the energy is sufficiently low, all of the axial kinetic energy is converted to rotational and radial energies, and particles are stopped axially and repelled back toward the anode. Since both $v_\theta$ and $v_r$ are proportional to r, the outermost particles suffer the most axial kinetic energy loss and are therefore more likely to be reflected. This is clearly seen in Figure 2(a). Overall, the beam focal point can clearly be seen to approach the aperture as energy increases. In particular, at the beam peak the focal point is near the aperture, with most particles passing through as can be seen in Figure 2(c). Except near the focal point where space charge and aberration effects play an important role, the results from numerical simulations and the linear analysis are generally in good agreement. The beam current trace measured at the downstream aperture is shown in Figure 3(b). Substantial risetime sharpening is observed in comparison with the original diode current.

## 3.2 DIODE WITH ANODE FOIL

The radial impulse produced by a conducting foil on a uniform current density profile electron beam has been determined by Adler.[9] Assuming that the foil produces a change in radial momentum $\delta p_r$ without a change in radial position (the thin lens approximation), the deflection angle of the electrons from the foil is given by

$$\delta\theta_f = \frac{\delta p_r}{p_z} = -16 \frac{I_b}{I_A} \frac{b}{a} \sum_{n=1}^{\infty} \frac{J_1\left( \chi_{0n} a/b \right) J_1\left( \chi_{0n} r/b \right)}{\chi_{0n}^3 J_1^2\left( \chi_{0n} \right)} , \tag{15}$$

where a is the beam radius at the foil, b is the drift tube wall radius, $\chi_{mn}$ is the nth root of $J_m$, and $I_A = 4\pi\epsilon_o mc^3\beta\gamma/e$ is the Alfven current. Equation (15) may be used as the initial condition on R′ to solve Equation (6).

The presence of the anode foil also enhances beam emittance through electron scattering. For electrons passing through $\eta_z L$ atoms/$m^2$ of atomic number Z, the cumulated mean squared scattering angle is[14]

$$\langle\theta_s^2\rangle = \frac{8\pi e^4 Z(Z+1)\eta_z L}{\left(4\pi\epsilon_o\right)^2 m^2\gamma^2\beta^4 c^4} \ell n \left( \frac{\theta_{max}}{\theta_{min}} \right) , \tag{16}$$

where, for the thin target case,

$$\left( \frac{\theta_{max}}{\theta_{min}} \right) = \frac{h}{\sqrt{\pi}\, mc\beta} Z^{2/3} \left( \eta_z L \right)^{1/2} . \tag{17}$$

The cathode surface roughness also contributes to the beam emittance as previously described analytically by Equation (10). Application of Equations (10) and (16) together give a reasonable approximation to the emittance of the electron beam emerging from the anode foil as compared with previous emittance measurements with a similar cathode. Equation (15) has been found to be a reasonable approximation to the foil-focusing effect based upon comparison with beam radius data taken with radiachromic films.

Since from the above analysis all the terms of the envelope equation are significant, Equation (5) becomes nonlinear and must be solved numerically.

From the resulting numerical solution, we can determine the focal point and the beam radius at the waist to allow appropriate placement of the downstream aperture.

To aid in the design of the experiment and to test the validity of the technique, numerical simulations of Equation (5) were performed assuming a 1.6 MV peak electron beam with 3.5 kA of injected current and an injection radius of 1.5 cm. The anode foil material was 6 μm thick aluminum. Typical numerical results are shown in Figures 4(a) and (b) for two different peak lens axial magnetic field strengths.

The figures illustrate the variation in the beam envelope as a function of beam energy. Figure 4(a) indicates that for peak lens magnetic fields on the order of 1.2 kG, the lower energy portion of the beam is brought to a focus a reasonable distance downstream of the lens center. The magnetic field strength however is insufficient to bring the high energy portion of the beam to a focus and it continues to expand radially. Aperturing the beam at a 1.5 cm radius, 15 cm downstream of the magnetic lens should then give us an output current pulse containing a large portion of the current emitted during the rising and falling edges of the voltage pulse, and a reduced current at the higher energies emitted near the peak of the diode voltage pulse. At stronger peak lens magnetic field strengths, the high energy portion of the beam is brought to a focus downstream of the lens center as shown in Figure 4(b). In this case the low energy portions of the beam current have been brought to a focus much closer to the lens center and have rapidly expanded downstream. As a result, very little of the low energy beam current will pass through the downstream aperture. This should result in a sharper rise to beam current peak. Figures 4(a) and (b) illustrate that by suitable selection of the peak lens magnetic field, significant current pulse shaping should be achievable. The implementation is not quite as straightforward as Figure 4 suggests since for the lower energy electrons there will actually be less current extracted from the cathode which is not accounted for in the simulation. This analysis also neglects nonlinear effects due to the magnetic lens which introduce a high transverse energy component to the beam.

# SECTION 4

# EXPERIMENTAL SETUP

The experimental configuration for investigating current pulse-shaping with the single magnetic lens is shown schematically in Figure 5. The electron beam is generated from a field emission cathode with a 0.9 cm radius velvet emitting surface. The anode consists of a stainless steel aperture plate with a 1.5 cm radius aperture. The anode-cathode gap spacing is approximately 2.5 cm. In this configuration, the Febetron 705 generates a nominal 2 MV, 7 kA, 20 ns (FWHM) electron beam in the diode. Experiments were attempted initially without an anode foil covering the aperture. In this case however, without an external magnetic field to confine the electrons emitted from the cathode, insufficient current was extracted through the aperture (on the order of 1.5 kA) to make the technique practical. The poor emission properties were attributed primarily to shank emission from the cathode stalk not accounted for in the MAGIC simulations. With an anode foil in place, extracted currents reached 4 kA through the anode aperture. Subsequent experiments used either a 6 μm aluminized mylar foil or a 15 μm titanium foil covering the anode aperture. The markedly different effect of the emittance of the electron beam extracted from the anode due to scattering in these two foils on the pulse-shaping properties of the magnetic lens cell could then be investigated.

The diode voltage is monitored with a capacitive voltage divider located upstream of the cathode stalk. The electron beam current injected into the pulse-shaping cell is monitored with a Rogowski coil immediately downstream of the anode. The magnetic lens, described in detail in Section 2, slides over the 6" diameter drift tube and is typically centered 20 cm downstream from the anode. A range-thick carbon aperture plate (1.5 cm radius aperture) is located typically 15 cm downstream from the center of the magnetic lens to extract only the desired portion of the electron beam. The beam current extracted through this aperture is monitored by a resistive wall current monitor

(beambug).[15] Further downstream from the aperture the beam current is monitored by a Faraday cup to monitor beam expansion. Alternatively, on some shots the time resolving electron energy spectrometer (TREES)[16] is placed downstream to get additional temporal information on the beam current and energy. This device is basically a compact magnetic spectrometer[17] with a fast detector. The device is intrusive in that it must be placed in the path of the electron beam. Typically the detector has been a fast scintillator or a plastic Cerenkov radiator. A streak camera images the light from the detector to give time-resolved information on the electron energy in the current pulse. A plastic film holder also allows positioning of an array of three radiachromic films over an axial length of 25 cm to allow for monitoring of the radial profile of the electron beam from the anode foil back to the carbon aperture. The entire diode and drift tube region is evacuated to $10^{-5}$ Torr by an oil diffusion pump.

# SECTION 5

## EXPERIMENTAL RESULTS AND DISCUSSION

The experiment was conducted using both the 15 μm thick titanium and the 6 μm aluminized mylar anode foils. Experimental results are shown in Figure 6 for both types of foil. Typical diode voltages are on the order of 1.7 MV. The diode current (not shown in Figure 6) has a peak value of about 7 kA and follows the diode voltage very closely in pulse shape. Beam current extracted through the anode aperture is more triangular in shape with peak values near 4 kA. The data in Figure 6 shows the results from both foils to have the same trend in variation of pulse shape with peak lens magnetic field with one important difference. The peak current obtained with the titanium foil is much less than that obtained with the aluminized mylar foil. While a maximum of 90 percent of the beam current extracted from the anode is transported through the pulse shaping cell using the aluminized mylar foil, only about 50 percent is effectively transported using the thicker titanium foil at a reduced peak magnetic field. This is likely a result of the combined effect of electron energy loss in the titanium and increased transverse temperature due to enhanced scattering.

The results demonstrate the effects anticipated by the simple envelope equation analysis of Section 3. For relatively low peak magnetic field strengths, the lower energy portion of the beam is focused through the downstream carbon aperture. The higher energy portion of the beam is not focused and as a result transports less current through the aperture. By increasing the magnetic field strength of the lens appropriately the beam current pulse can be made reasonably square (6 ns rise and fall times (10-90%) with a 12 ns flattop). Further increasing the peak magnetic field allows more of the peak beam current to pass through the carbon aperture with less of the low-energy components but at a somewhat slower risetime.

Information has also been obtained using the TREES that is useful in

illustrating this result. Figures 7(a) and (b) show streak photographs obtained with the TREES located downstream of the carbon aperture plate using the 15 μm thick titanium anode foil. In Figure 7(a), with no magnetic field applied, the image appears spread out over 19 ns with a definite increase in intensity near the center of the trace. In Figure 7(b), with a peak axial magnetic field of 1.6 kG, the trace appears to be shorter, spread out over 14 ns, but more importantly is uniform in intensity. This indicates that the lower energy (lower current) portion of the beam did not make it through the aperture to be intercepted by the TREES.

# SECTION 6

# CONCLUSIONS

The experimental results indicate that the single magnetic lens is an effective tool for shaping the output beam current pulse. Experiments conducted with a nonmagnetized foilless diode were not successful due primarily to degraded emission characteristics from the cathode and cathode shank. For diode configurations employing anode foils, the results are qualitatively in good agreement with the simulation results from the beam envelope equation analysis. Although the presence of the anode foil introduces foil focusing and the added transverse thermal spread due to electron scattering, the effectiveness of the magnetic lens is substantial. The added transverse energy spread limits the spot size attainable at the downstream focal point but for applications in which the electron beam is to be matched to a transport section (an IFR channel for example) with a radius comparable to the injection radius this should not be a problem.

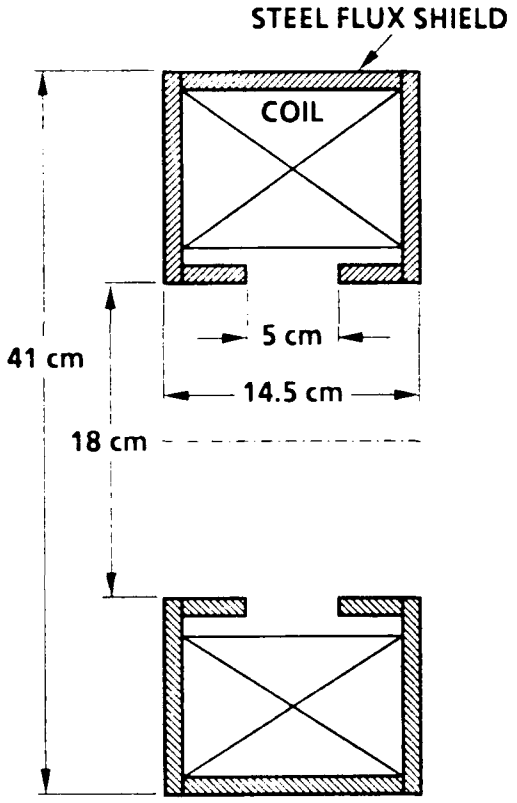


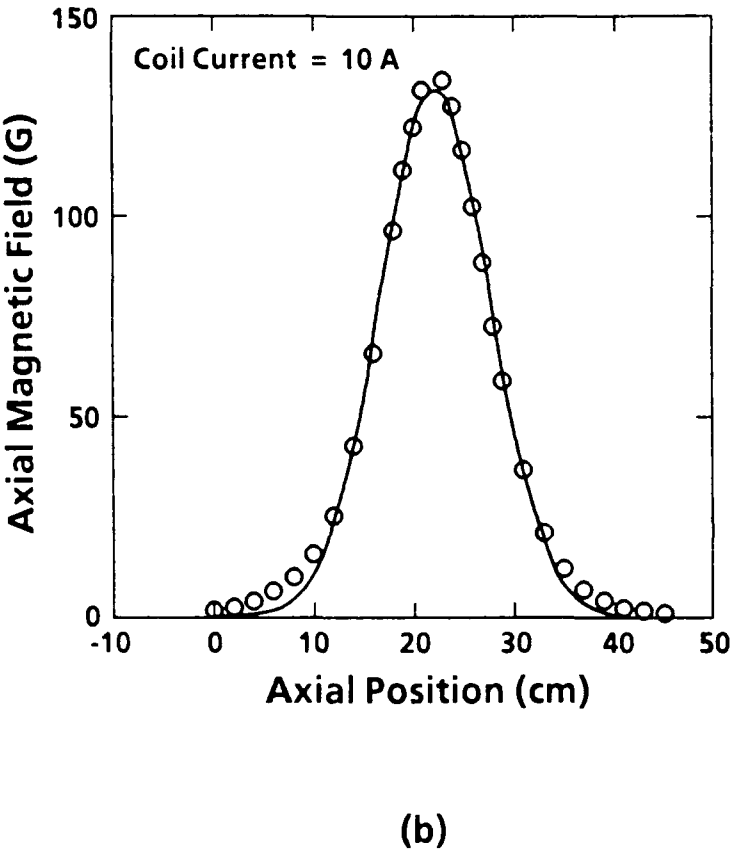


FIGURE 1A. SCHEMATIC OF THE MAGNETIC LENS

FIGURE 1B. AXIAL MAGNETIC FIELD PROFILE

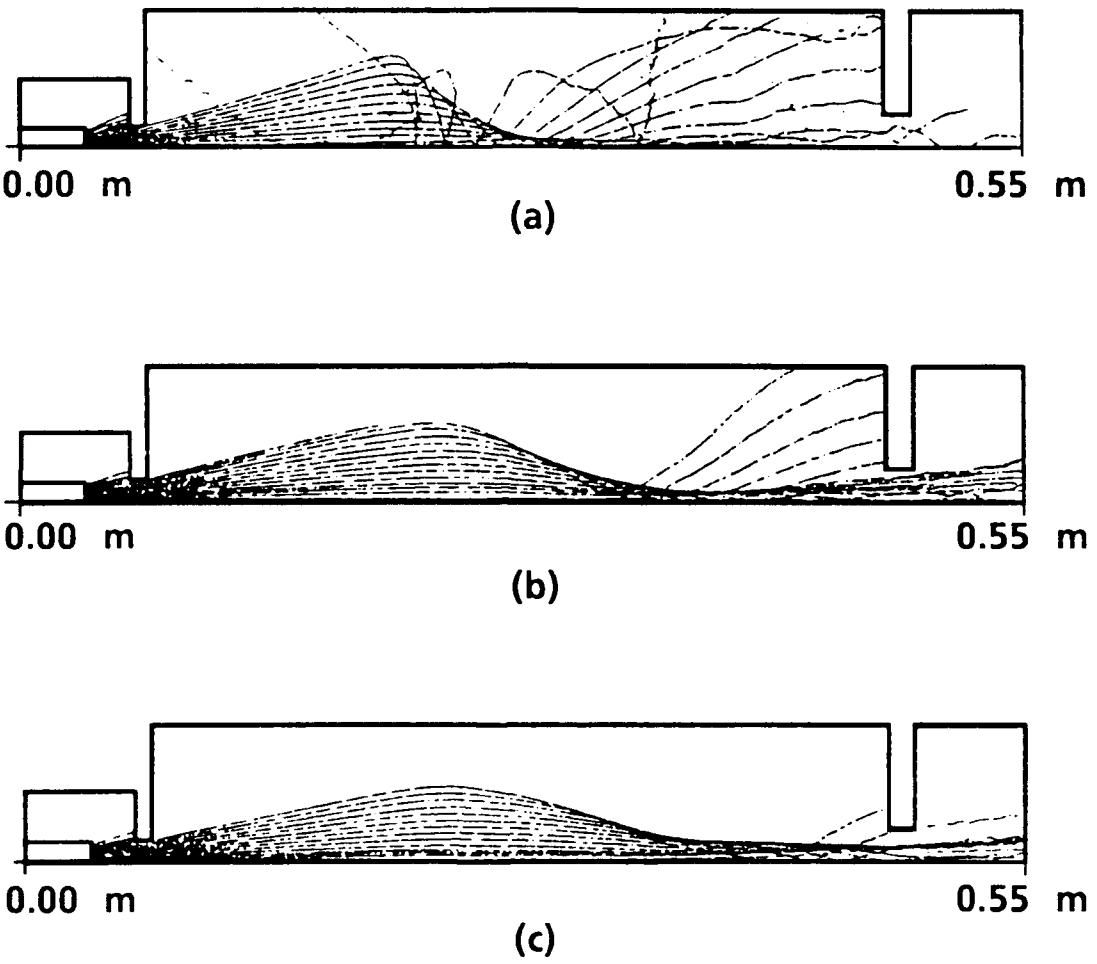


FIGURE 2. BEAM TRAJECTORY PLOT AT (A) 5.9 ns, (B) 12.5 ns, AND (C) 19.1 ns, FROM MAGIC SIMULATION

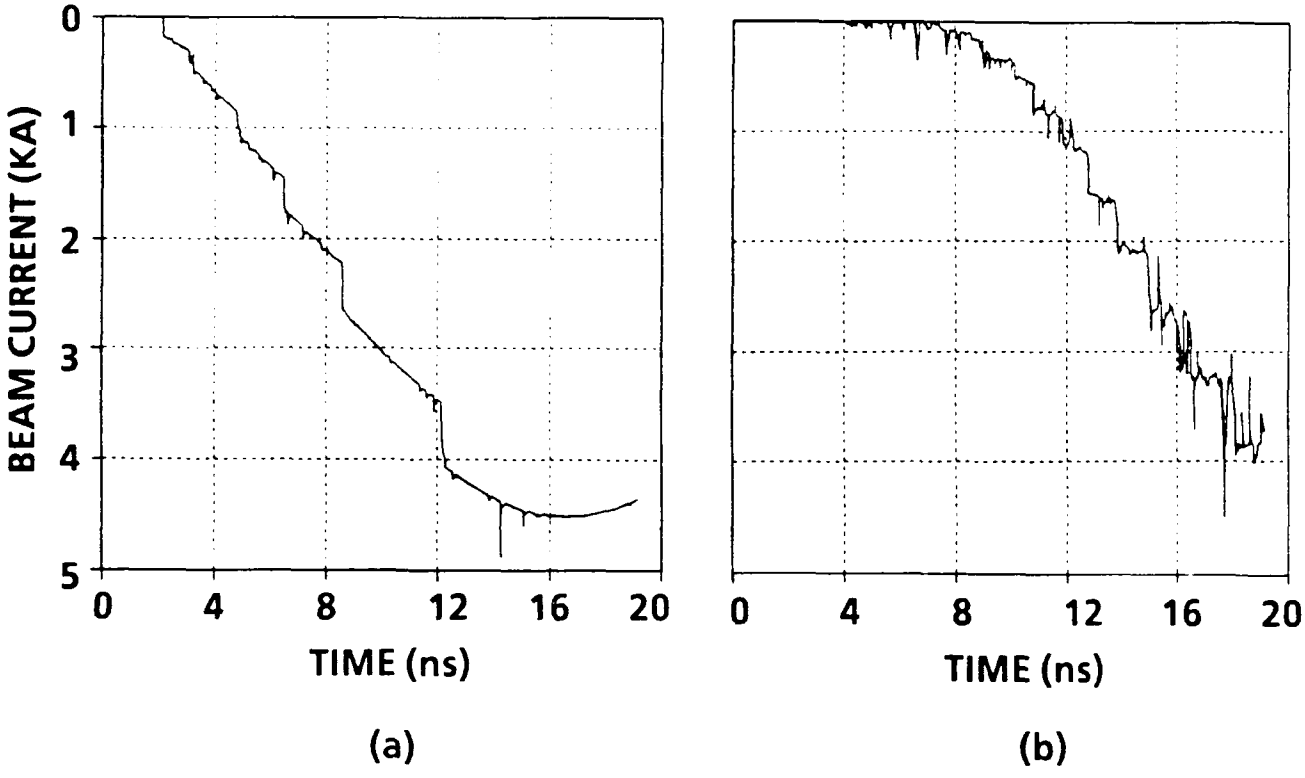


FIGURE 3A. TEMPORAL PROFILE OF BEAM CURRENT EXITING THE ANODE APERTURE

FIGURE 3B. TEMPORAL PROFILE OF THE SHARPENED BEAM CURRENT

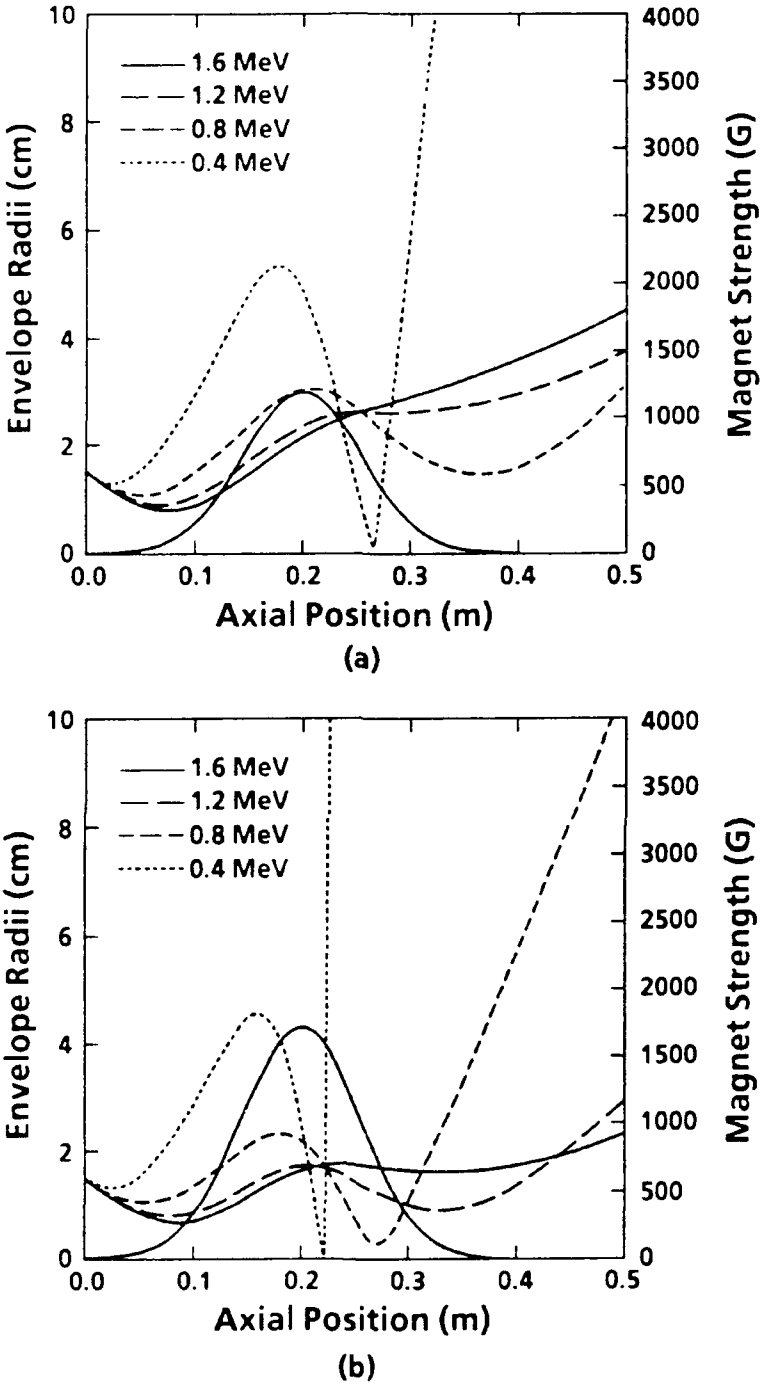


FIGURE 4. ENVFLOPE SOLUTION FOR PEAK LENS AXIAL MAGNETIC FIELD OF: (A) 1.17 kG AND (B) 1.69 kG

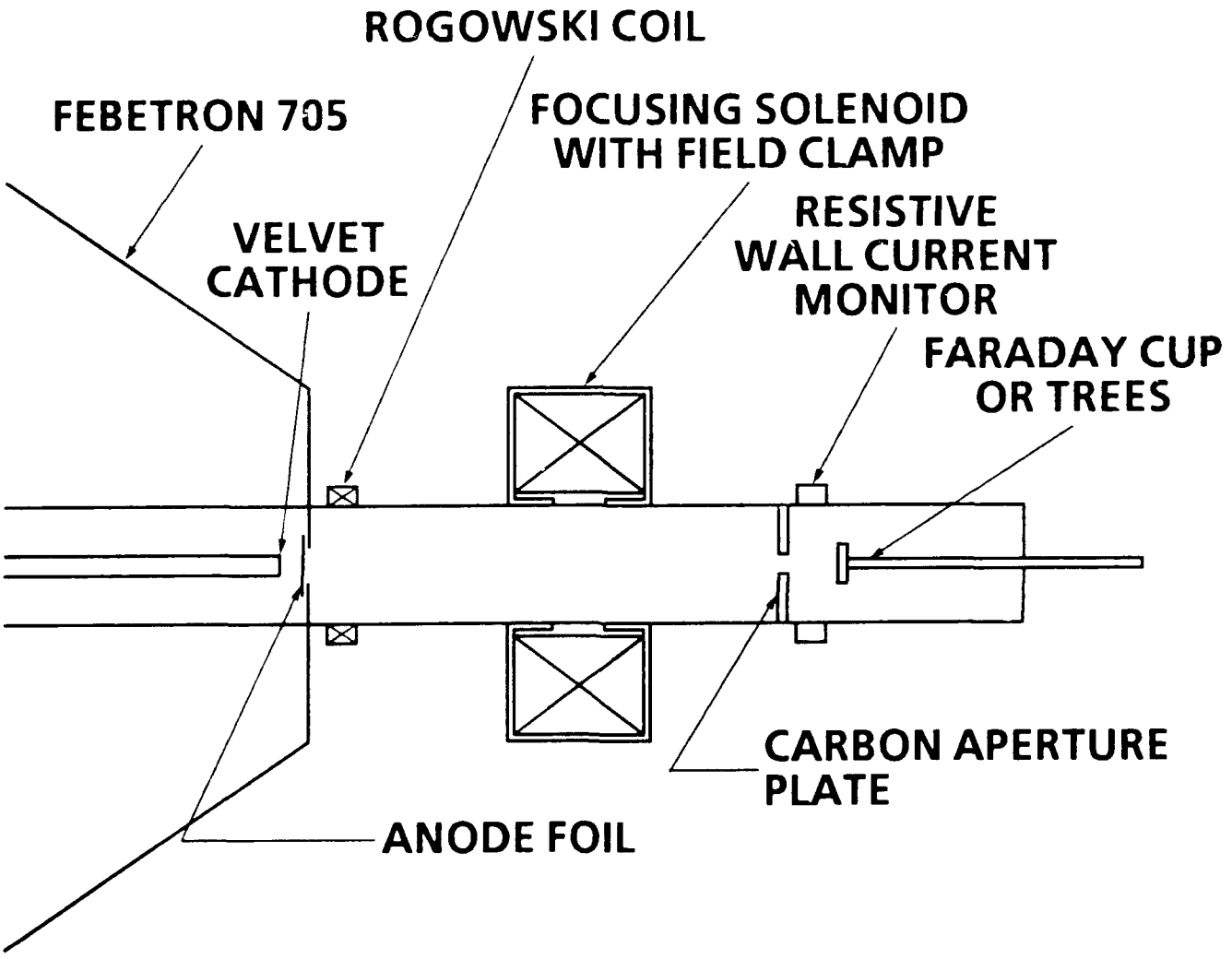


FIGURE 5. SCHEMATIC OF CURRENT PULSE SHAPING EXPERIMENT WITH A SINGLE MAGNETIC LENS

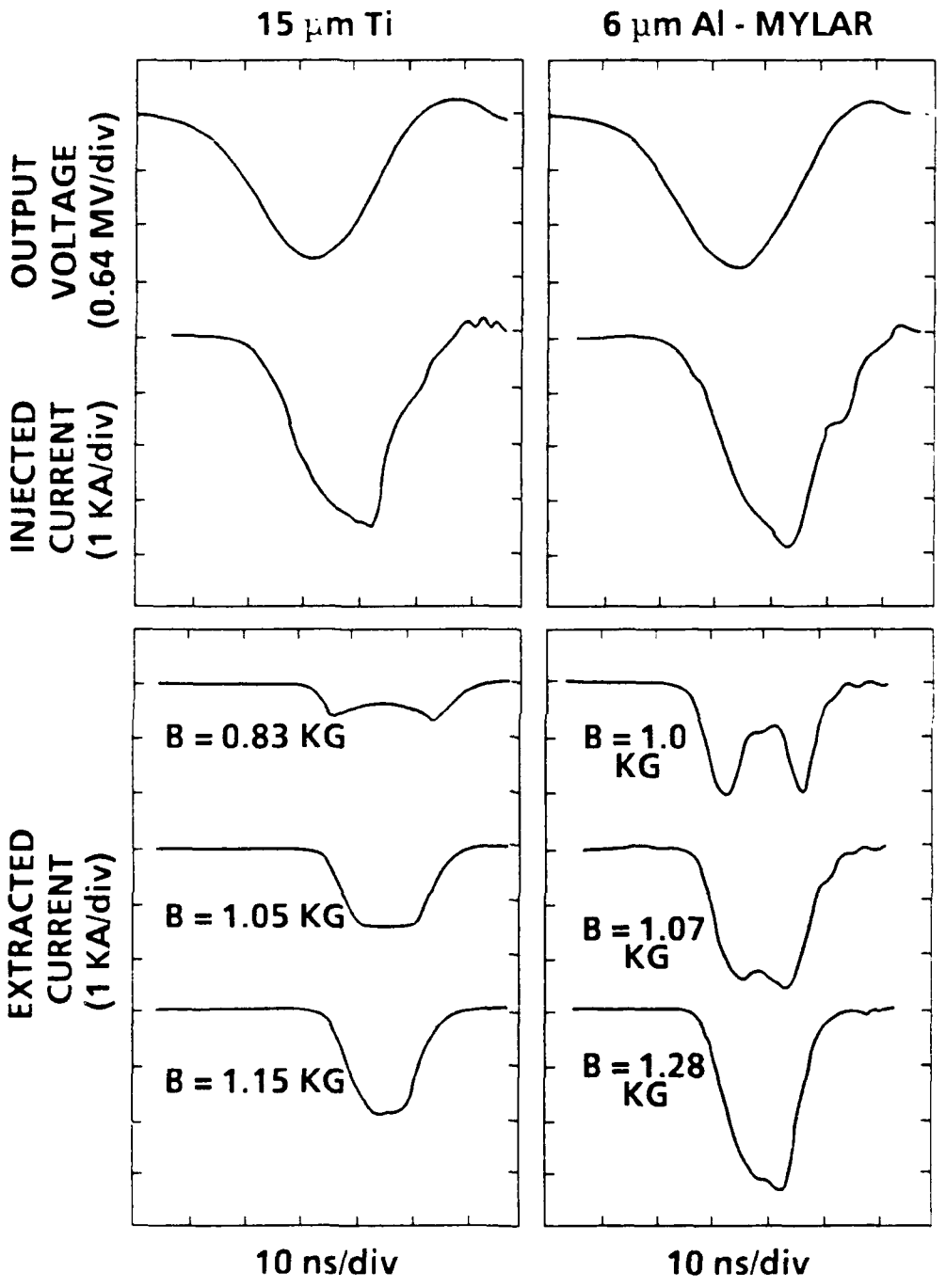


FIGURE 6. EXPERIMENTAL RESULTS FOR TWO DIFFERENT ANODE FOILS

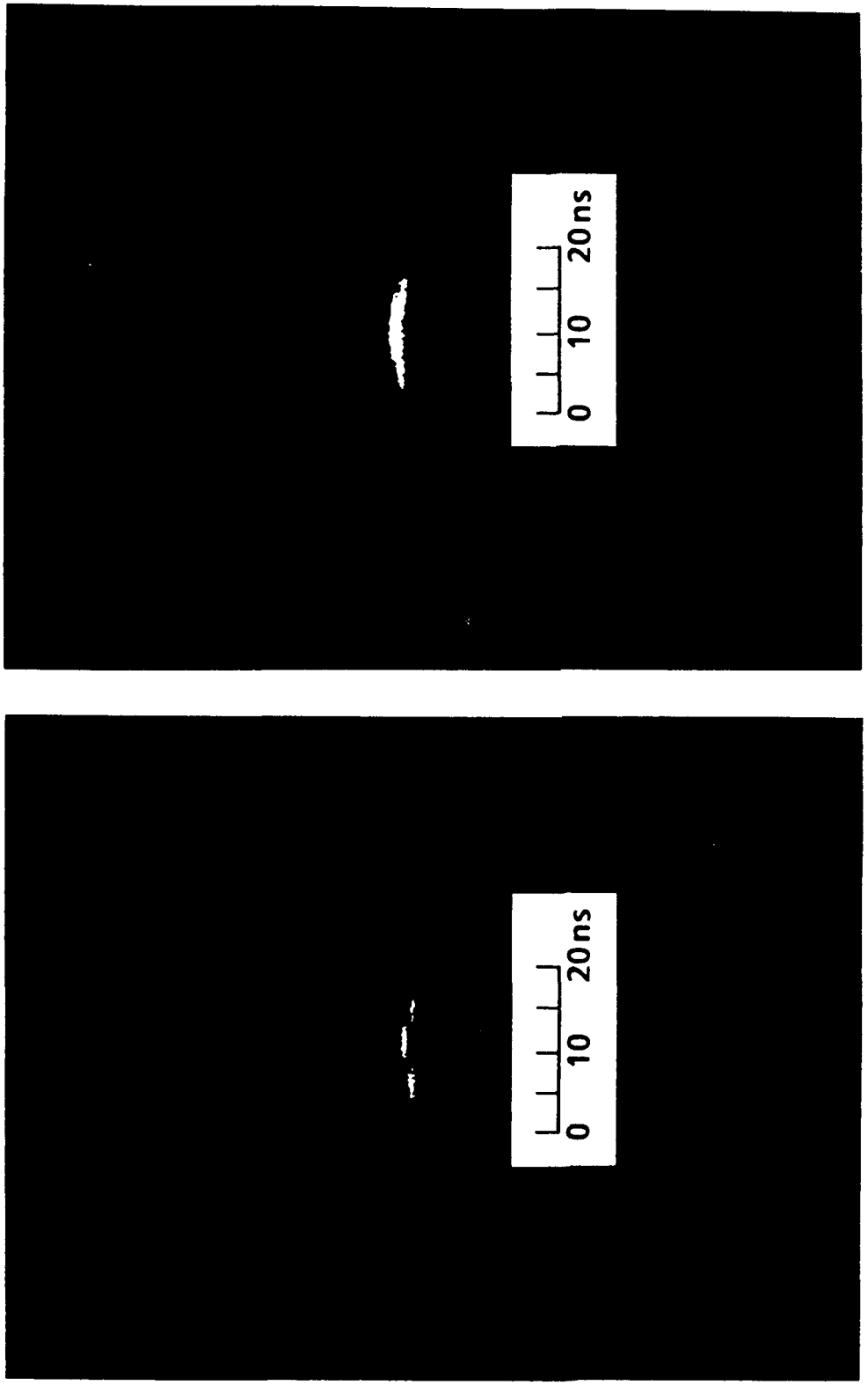


FIGURE 7. STREAK CAMERA PHOTOGRAPHS OF THE TREES USING THE 15 μm TITANIUM FOIL AND; (A) NO MAGNETIC FIELD, AND (B) PEAK FIELD OF 1.6 kG

## REFERENCES


1. Merkel, G., private communication.

2. Lidestri, J., private communication.

3. Parsons, C.R., Nolting, E.E., Kenyon, V.L., Smith, R.A., Genuario, R.D., and Bailey, V.L., "IREB Transport and Risetime Compression Using Magnetic Field Gradients," Digest of Technical Papers of the 4th IEEE Pulsed Power Conference, Albuquerque, NM, catalog #83CH1908-3, (IEEE, New York, 1983), p 498.

4. Lee, J.R., Backstrom, R.C., Halbleib, J.A., Quintenz, J.P., and Wright, T.P., "Gradient B Drift Transport of High Current Electron Beams," J. Appl. Phys., Vol. 56, 1984, p. 3175; Lee, J.R., "Pulse Shaping of High-Current Electron Beams with Gradient B Drift Transport," Sandia National Laboratory Report SNAD86-0920, Albuquerque NM , 1986, unpublished.

5. Lawson, J.D., The Physics of Charged Particle Beams, (Oxford University Press, Oxford, 1977).

6. Loschialpo, P., Namkung, W., Reiser, M., and Lawson, J.D., "Effects of Space-Charge and Lens Aberrations in the Focusing of an Electron Beam by a Solenoid Lens," J. Appl. Phys., Vol. 57, 1984, p. 10.

7. Bekefi, G., Hartemann, F., and Kirkpatrick, D.A., "Temporal Evolution of Beam Emittance from a Field Emission Electron Gun," J. Appl. Phys., Vol. 62, 1987, p. 1564.

8. Adler, R.J., and Miller, R.B., "A Pinch Effect for Intense Magnetized, Non-Neutral Electron Beams," J. Appl. Phys., Vol. 53, 1982, p. 6015.

9. Adler, R.J., "Image-Field Focusing of Intense Ultra-Relativistic Electron Beams in Vacuum," Part. Accel., Vol. 12, 1982, p. 263.

10. Humphries, S., Jr., Ekdahl, C., and Woodall, D.M., "Image Current Guiding of a Relativistic Electron Beam in a Foil Focusing System," Appl. Phys. Lett., Vol. 54, 1989, p. 2195.

11. Nguyen, K.T., "Febetron Rise Time Sharpening With Magnetic Lens," Mission Research Corporation Report MRC/WDC-R-221, Newington, VA, 1990, unpublished.

12. Lau, Y.Y., "Effects of Cathode Surface Roughness on the Quality of

Electron Beams," J. Appl. Phys., Vol. 61, 1987, p. 36.

13. Goplen, B., Ludeking, L., McDonald, J., Warren, G., and Worl, R., "MAGIC User's Manual," Mission Research Corporation Report MRC/WDC-R-216, 1989, unpublished.

14. Lauer, E.J., "Universal Curves for Predicting Equilibrium Radii of Relativistic Electron Beams Including the Effects of Attractive Self Force, External $B_z$, Initial Beam Quality and Scattering in the Gas Entry Foil," Lawrence Livermore National Laboratory Report UCID-16716, 1975, unpublished.

15. Struve, K.W., "Electrical Measurement Techniques for Pulsed High Current Electron Beams," Conference Record of the Workshop on Measurement of Electrical Quantities in Pulse Power Systems II, IEEE Catalog No. 86CH2327-5, 1986, p. 36.

16. Weidman, D.J., Rhee, M.J., and Schneider, R.F., "Preliminary Experimental Results from the Time-Resolving Electron Energy Analyzer," Bull. Am. Phys. Soc., Vol. 35, 1989, p. 1005.

17. Schneider, R.F., Luo, C.M., Rhee, M.J., and Smith, J.R., "Compact Magnetic Electron Energy Analyzer," Rev. Sci. Instrum., Vol. 56, 1985, p. 1534.

18. Jackson, J.D., Classical Electrodynamics, (Wiley, New York, 1975).

# APPENDIX

## RADIAL IMPULSE IN A FOILLESS DIODE

We note that in the case where the anode foil is in place, the potential along the diode axis can be well represented by

$$\phi(r=0,z) = -V\left(1-z/d\right) \tag{A1}$$

where V is the diode voltage and d is the distance between the cathode and anode. If a small hole of radius a (a<d) is introduced, then the potential in Eq. (A1) can be modified to be[18]

$$\phi(0,z) = \begin{cases} -V\left(1-\dfrac{z}{d}\right) - \dfrac{Va}{\pi d}\left[1+\dfrac{z-d}{d}\,\mathrm{Atan}\left(\dfrac{a}{d-z}\right)\right], & 0 \le z \le d \\ \dfrac{Va}{\pi d}\left[1-\dfrac{z-d}{a}\,\mathrm{Atan}\left(\dfrac{a}{z-d}\right)\right], & z \ge d \end{cases} \tag{A2}$$

The result on the axial electric field is given by

$$E_z(0,z) \simeq \begin{cases} -\dfrac{V}{d}+\dfrac{V}{\pi d}\left[\mathrm{Atan}\left(\dfrac{a}{d-z}\right)+\dfrac{a(z-d)}{(z-d)^2+a^2}\right], & 0 \le z \le d \\ \dfrac{V}{\pi d}\left[-\mathrm{Atan}\left(\dfrac{a}{z-d}\right)+\dfrac{a(z-d)}{(z-d)^2+a^2}\right], & z \ge d \end{cases} \tag{A3}$$

Then the radial field in the diode structure can be approximated by

$$E_r(r,z) \simeq -\frac{1}{2}\,r\,\frac{\partial E_z}{\partial z} = -\,r\,\frac{V}{\pi d}\,\frac{a^3}{\left[(z-d)^2+a^2\right]^2}, \qquad z \ge 0. \tag{A4}$$

The above equation indicates that the radial electric field is sharply peaked at the anode.

Thus, most of the transverse momentum gain is expected to occur near the anode aperture where electrons move near the speed of light for the range of voltage considered. Then the electron radial equation of motion can be approximated by

$$\frac{d\left(\gamma v_r\right)}{dz} = -\frac{e}{mv_z} E_r \tag{A5}$$

The sharply peaked radial electric field means the radial position changes relatively little across the aperture gap. Integrating Eq. (A5) across the aperture region, we obtain the electron radial impulse due to the aperture

$$r' = \frac{v_r}{v_z} = \frac{eV}{\gamma m v_z^2} \frac{r}{2d} = \frac{\gamma}{\gamma+1} \frac{r}{2d} \tag{A6}$$

DISTRIBUTION

| | Copies |
|---|---|
| Strategic Defense Initiative Organization | |
| Attn: LTC M. Toole | 1 |
| MAJ P. O'Reilly | 1 |
| Directed Energy Office | |
| The Pentagon | |
| Washington, DC 20301-7100 | |
| Defense Advanced Research Projects Agency | |
| Attn: Dr. H. Lee Buchanan | 1 |
| Dr. B. Hui | 1 |
| Directed Energy Office | |
| 1400 Wilson Boulevard | |
| Arlington, VA 22209-2308 | |
| Commander | |
| Naval Sea Systems Command | |
| Attn: Mr. D. L. Merritt | 1 |
| LCDR W. Fritchie | 1 |
| Code PMW 145 | |
| Washington, DC 20363-5100 | |
| Defense Technical Information Center | |
| Cameron Station | |
| Alexandria, VA 22304-6145 | 12 |
| Library of Congress | |
| Attn: Gift and Exchange Division | 4 |
| Washington, DC 20549 | |
| Commander | |
| Harry Diamond Laboratories | |
| Attn: Mr. S. Graybill | 1 |
| Dr. G. Merkel | 1 |
| Branch 2290C | |
| 2800 Powder Mill Road | |
| Adelphi, MD 20783 | |

| | Copies |
|---|---|
| Commanding Officer | |
| Naval Research Laboratory | |
| Attn: Code 4790 (Dr. G. Joyce) | 1 |
| Code 4790 (Dr. M. Lampe) | 1 |
| Code 4750 (Dr. R. Meger) | 1 |
| Code 4750 (Dr. R. Pechacek) | 1 |
| Code 4751 (Dr. D. Murphy) | 1 |
| 4555 Overlook Avenue, SW | |
| Washington, DC 20375 | |
| Mission Research Corporation | |
| Attn: Dr. K. T. Nguyen | 1 |
| Dr. J. Pasour | 1 |
| 8560 Cinderbed Road, Suite 700 | |
| Newington, VA 22122 | |
| Mission Research Corporation | |
| Attn: Dr. K. W. Struve | 1 |
| Dr. D. Welch | 1 |
| 1720 Randolph Road, SE | |
| Albuquerque, NM 87106 | |
| Defense Nuclear Agency | |
| Attn: Dr. R. L. Gullickson | 1 |
| 6801 Telegraph Road | |
| Alexandria, VA 22310 | |
| Air Force Weapons Laboratory | |
| Kirtland Air Force Base | |
| Attn: Dr. B. Godfrey | 1 |
| Albuquerque, NM 87117-6008 | |
| Titan Technologies | |
| Spectron Division | |
| Attn: Dr. R. B. Miller | 1 |
| Dr. J. R. Smith | 1 |
| 2017 Yale Blvd., SE | |
| Albuquerque, NM 87106 | |

| | Copies |
|---|---|
| Pulse Sciences, Inc. | |
| Attn: Dr. S. D. Putnam | 1 |
| 14796 Wicks Blvd. | |
| San Leandro, CA 94577 | |
| | |
| University of Maryland | |
| Attn: Dr. M. J. Rhee | 1 |
| Dr. W. W. Destler | 1 |
| Dr. M. P. Reiser | 1 |
| Dr. J. Goldhar | 1 |
| Electrical Engineering Dept. | |
| College Park, MD 20742 | |
| | |
| Lawrence Livermore Laboratory | |
| Attn: Dr. D. Prosnitz | 1 |
| Dr. F. W. Chambers | 1 |
| Dr. T. Orzechowski | 1 |
| P.O. Box 808 | |
| Livermore, CA 94550 | |
| | |
| Los Alamos National Laboratory | |
| Attn: Dr. R. Carlson | 1 |
| Dr. D. Moir | 1 |
| Dr. C. Ekdahl | 1 |
| Dr. P. O'Shea | 1 |
| P.O. Box 1663 | |
| Los Alamos, NM 87545 | |
| | |
| Sandia National Laboratory | |
| Attn: Div. 1272 | |
| Dr. M. Mazarakis | 1 |
| Dr. S. Shope | 1 |
| Div. 1274 | |
| Dr. R. Lipinski | 1 |
| Dr. C. Frost | 1 |
| P.O. Box 5800 | |
| Albuquerque, NM 87185 | |
| | |
| The University of Michigan | |
| Attn: Dr. R. M. Gilgenbach | 1 |
| Nuclear Engineering Dept. | |
| Ann Arbor, MI 48109 | |

| Internal Distribution: | Copies |
|---|---|
| R | 1 |
| R40 | 1 |
| R401 (G. Nolting) | 1 |
| R42 | 1 |
| R42 (H. Uhm) | 1 |
| R42 (R. F. Schneider) | 1 |
| R42 (D. Rule) | 1 |
| R42 (R. Fiorito) | 1 |
| R42 (R. Chen) | 1 |
| R42 (R. Stark) | 1 |
| R42 (W. Freeman) | 1 |
| R42 (M. Moffatt) | 1 |
| R42 (J. Choe) | 1 |
| R42 (K. Boulais) | 1 |
| R42 (J. Miller) | 15 |
| R42 (D. Weidman) | 1 |
| E231 | 2 |
| E232 (Chair Heritage) | 3 |

# REPORT DOCUMENTATION PAGE

Form Approved
OMB No 0704-0188



| 1. AGENCY USE ONLY (Leave blank) | 2. REPORT DATE | 3. REPORT TYPE AND DATES COVERED |
|---|---|---|
| | 28 June 1990 | Technical Report 10/89 to 7/90 |

**4. TITLE AND SUBTITLE**
Pulse Shaping a High-Current Relativistic Electron Beam in Vacuum

**5. FUNDING NUMBERS**
PR 0R40CA505

**6. AUTHOR(S)**
J. D. Miller, R. F. Schneider, and H. S. Uhm (NAVSWC), K. T. Nguyen and K. W. Struve (Mission Research Corp.), and D. J. Weidman (Advanced Technology and Research)

**7. PERFORMING ORGANIZATION NAME(S) AND ADDRESS(ES)**
Naval Surface Warfare Center
White Oak Laboratory
10901 New Hampshire Avenue
Silver Spring, MD 20903-5000

**8. PERFORMING ORGANIZATION REPORT NUMBER**
NAVSWC TR 90-268

**9. SPONSORING MONITORING AGENCY NAME(S) AND ADDRESS(ES)**
Strategic Defense Initiative Office of Directed Energy
The Pentagon
Office of the Secretary of Defense
Washington, DC 20301-7100

**10. SPONSORING / MONITORING AGENCY REPORT NUMBER**

**11. SUPPLEMENTARY NOTES**

**12a. DISTRIBUTION AVAILABILITY STATEMENT**
Approved for public release; distribution is unlimited.

**12b. DISTRIBUTION CODE**

**13. ABSTRACT** (Maximum 200 words)

A simple method for shaping the output current pulse of a relativistic electron beam in vacuum is presented. This method has been employed to sharpen the risetime of a high-current relativistic electron beam produced by a 2 MV, 7 kA, 20 ns pulser. The beam nominally has a pulse shape that is triangular in both voltage and current, with a negligible instantaneous energy spread. The desired pulse shape is nominally rectangular in current. The technique utilizes a magnetic lens with a magnitude of approximately 1.5 kG to focus the beam. Passing beam electrons through the magnetic lens causes them to focus at different axial locations downstream from the lens depending upon their energy. The focal point of the beam current peak (corresponding to maximum energy) is then located furthest downstream. An aperture is used near the focus to select a portion of the beam having the desired parameters.

**14. SUBJECT TERMS**
electron beam
pulse shaping
magnetic lens
risetime sharpening

**15. NUMBER OF PAGES**
37

**16. PRICE CODE**

| 17. SECURITY CLASSIFICATION OF REPORT | 18. SECURITY CLASSIFICATION OF THIS PAGE | 19. SECURITY CLASSIFICATION OF ABSTRACT | 20. LIMITATION OF ABSTRACT |
|---|---|---|---|
| UNCLASSIFIED | UNCLASSIFIED | UNCLASSIFIED | UNLIMITED |

## GENERAL INSTRUCTIONS FOR COMPLETING SF 298

The Report Documentation Page (RDP) is used in announcing and cataloging reports. It is important that this information be consistent with the rest of the report, particularly the cover and title page. Instructions for filling in each block of the form follow. It is important to ***stay within the lines*** to meet ***optical scanning requirements***.

**Block 1.** Agency Use Only *(Leave blank)*.

**Block 2.** Report Date. Full publication date including day, month, and year, if available (e.g. 1 Jan 88). Must cite at least the year.

**Block 3.** Type of Report and Dates Covered. State whether report is interim, final, etc. If applicable, enter inclusive report dates (e.g. 10 Jun 87 - 30 Jun 88).

**Block 4.** Title and Subtitle. A title is taken from the part of the report that provides the most meaningful and complete information. When a report is prepared in more than one volume, repeat the primary title, add volume number, and include subtitle for the specific volume. On classified documents enter the title classification in parentheses.

**Block 5.** Funding Numbers. To include contract and grant numbers; may include program element number(s), project number(s), task number(s), and work unit number(s). Use the following labels:

| | | | |
|---|---|---|---|
| **C** | - Contract | **PR** | - Project |
| **G** | - Grant | **TA** | - Task |
| **PE** | - Program Element | **WU** | - Work Unit Accession No. |

**Block 6.** Author(s). Name(s) of person(s) responsible for writing the report, performing the research, or credited with the content of the report. If editor or compiler, this should follow the name(s).

**Block 7.** Performing Organization Name(s) and Address(es). Self-explanatory.

**Block 8.** Performing Organization Report Number. Enter the unique alphanumeric report number(s) assigned by the organization performing the report.

**Block 9.** Sponsoring/Monitoring Agency Name(s) and Address(es). Self-explanatory.

**Block 10.** Sponsoring/Monitoring Agency Report Number *(If known)*.

**Block 11.** Supplementary Notes. Enter information not included elsewhere such as: Prepared in cooperation with ...; Trans. of ...; To be published in .... When a report is revised, include a statement whether the new report supersedes or supplements the older report.

**Block 12a.** Distribution/Availability Statement. Denotes public availability or limitations. Cite any availability to the public. Enter additional limitations or special markings in all capitals (e.g. NOFORN, REL, ITAR).

- **DOD** - See DoDD 5230.24, "Distribution Statements on Technical Documents."
- **DOE** - See authorities.
- **NASA** - See Handbook NHB 2200.2.
- **NTIS** - Leave blank.

**Block 12b.** Distribution Code.

- **DOD** - Leave blank.
- **DOE** - Enter DOE distribution categories from the Standard Distribution for Unclassified Scientific and Technical Reports.
- **NASA** - Leave blank.
- **NTIS** - Leave blank.

**Block 13.** Abstract. Include a brief *(Maximum 200 words)* factual summary of the most significant information contained in the report.

**Block 14.** Subject Terms. Keywords or phrases identifying major subjects in the report.

**Block 15.** Number of Pages. Enter the total number of pages.

**Block 16.** Price Code. Enter appropriate price code *(NTIS only)*.

**Blocks 17. - 19.** Security Classifications. Self-explanatory. Enter U.S. Security Classification in accordance with U.S. Security Regulations (i.e., UNCLASSIFIED). If form contains classified information, stamp classification on the top and bottom of the page.

**Block 20.** Limitation of Abstract. This block must be completed to assign a limitation to the abstract. Enter either UL (unlimited) or SAR (same as report). An entry in this block is necessary if the abstract is to be limited. If blank, the abstract is assumed to be unlimited.